Lithium-ion batteries are experiencing a huge surge in demand for electric vehicle and grid storage applications. To reduce the cost of batteries in these technologies there is a continual push to improve the energy density of the cells. Replacing the conventional graphite anode with lithium metal is one of the most popular approaches, as this can increase the cell energy density by 40–50% (refs. [1,2]). However, this substantial increase in cell energy is achieved only if the excess thickness of the lithium anode is limited [1,3]. Unfortunately, lithium-metal cells reported in the literature often use extremely thick anodes containing over 10 times the amount of lithium actually being cycled. This huge excess could never be used in a practical cell and makes interpretation of results more difficult, as cycling stability becomes artificially enhanced. As a result, researchers have called for limiting the lithium excess to less than 50 μm (ref. [4]).

Limiting lithium excess is a challenge, as lithium metal is prone to form dendrites with high surface area, which reduce cycling efficiency by increasing the reactivity of the anode with the electrolyte and forming isolated metallic lithium [5–7]. The low cycling stability of lithium metal is especially apparent in the anode-free or zero-excess configuration, where cells are built with a bare copper anode and the lithium is plated directly from the cathode on the first charge cycle [8–12]. Since there is no excess lithium built into the cell, volume is minimized (Fig. 1a) and energy density is maximized [1,3,4], but performance may be very poor since there is no reservoir of fresh lithium to replenish the cell during cycling. For example, Cu//NMC111

[1]Materials Engineering, Department of Mechanical Engineering, Dalhousie University, Halifax, Nova Scotia, Canada. [2]Tesla Canada R&D, Dartmouth, Nova Scotia, Canada. [3]Physics and Atmosphere Science, Dalhousie University, Halifax, Nova Scotia, Canada. [4]Nanotechnology Engineering, University of Waterloo, Waterloo, Ontario, Canada. [5]These authors contributed equally: R. Weber, M. Genovese. *e-mail: jeff.dahn@dal.ca

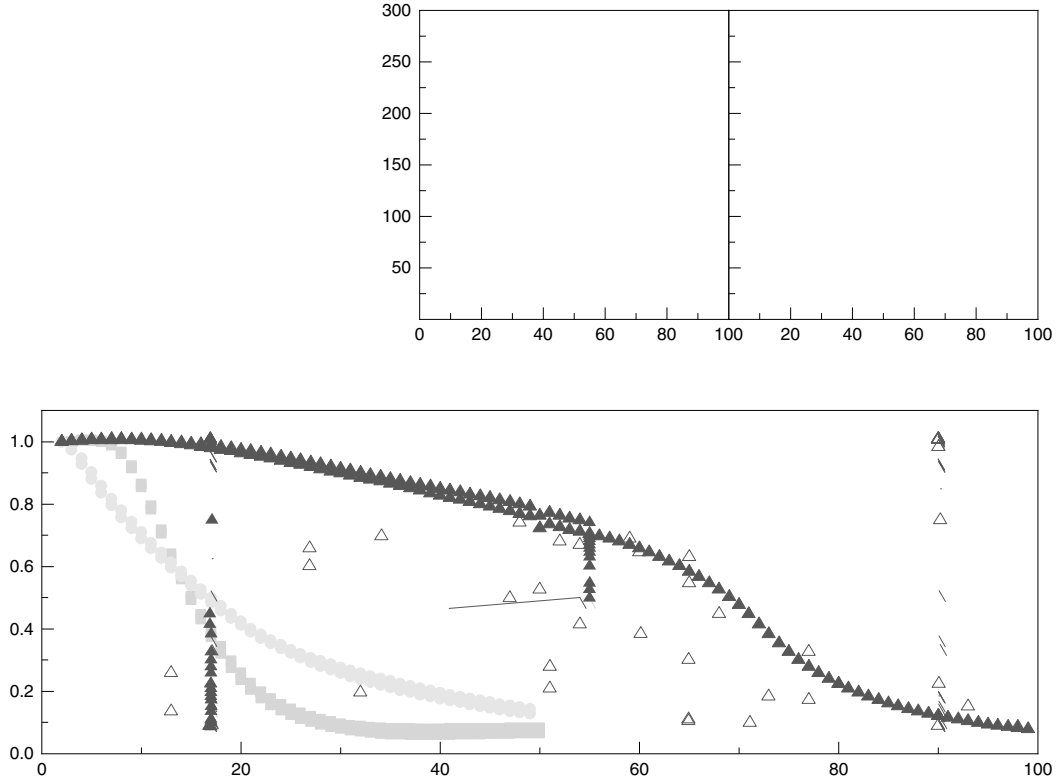

low uniaxial pressure (~75 kPa) applied to the cell stack (the method to apply pressure is shown in Supplementary Fig. 1). It should also be noted that these cells are operating under a very lean electrolyte condition of approximately 2 Ah $^{-1}$. Capacity retention data are summarized in Fig. 1b. The 1 M $LiPF_6$ and 1 M $LiBF_4$ single-salt control cells clearly demonstrate the challenge of anode-free cycling, as they fall below 80% retention in fewer than 15 cycles. Cycling stability was dramatically improved with the 1 M LiDFOB single-salt electrolyte, which reaches 60 cycles before falling below 80% capacity. Improved lithium-metal cycling with LiDFOB has been reported by others, especially in combination with FEC[22].

More interesting still is what happens when an additional salt is added to this LiDFOB electrolyte. The light-blue triangles in Fig. 1b show the capacity retention of a 0.6 M single-salt LiDFOB electrolyte, which falls below 80% capacity just before 50 cycles. When 0.6 M $LiPF_6$ is added to this electrolyte there is little to no effect on the number of cycles to 80% retention, but the onset of 'rollover' or complete cell failure is extended, since rollover is caused by the consumption of LiDFOB during cycling[15]. With the addition of 0.6 M $LiBF_4$, however (dark-blue circles), there is a substantial jump-in initial capacity retention, with the cell making it to 80 cycles with 80% capacity, a considerable achievement for an anode-free configuration under low applied pressure with limited excess electrolyte. Cells with a more optimized dual-salt blend of 1 M LiDFOB and 0.2 M $LiBF_4$ made it to 90 cycles before dropping below 80% capacity.

The unique properties of this LiDFOB/$LiBF_4$ blend are further highlighted through a comparison of the single- and dual-salt electrolytes charged to varying upper cut-off voltage (Fig. 1c,d). Figure 1c shows the cycling performance of the 1 M single-salt LiDFOB electrolyte charged to 4.2, 4.3 or 4.5 V. Surprisingly, the capacity retention of single-salt LiDFOB cells improves with increasing upper cut-off voltage. Previous studies of LiDFOB electrolytes in lithium-metal cells cycled below 4.3 V (refs. [15,28,30]), so this high-voltage enhancement has not been reported before. The problem with this performance improvement is that the poor oxidative stability of LiDFOB causes it to produce a lot of gas when cycled above 4.3 V (Supplementary Fig. 2). It is also impractical to require a cell to be consistently cycled to the top of charge to maintain good performance. Although the capacity retention for the dual-salt LiDFOB/$LiBF_4$ blend is similar to that for 1 M LiDFOB when cycled to 4.5 V, the dual-salt LiDFOB/$LiBF_4$ blend has the added benefit that it maintains good cycling stability across varying upper cut-off voltage (Fig. 1d). The dual-salt blend also produces less gas, especially when charged only to 4.3 V (Supplementary Fig. 2). Since gassing is reduced for the LiDFOB/$LiBF_4$ blend, cells with 1 M LiDFOB and 0.2 M $LiBF_4$ were able to undergo 100 charge–discharge cycles. This was difficult for higher-concentration cells with only LiDFOB due to the large amount of gas produced. Cells were almost ruptured and could not remain in the test fixture.

The superior performance of the LiDFOB/$LiBF_4$ mixture is also demonstrated in the cycling behaviour of Li||Cu half-cells (Supplementary Fig. 3). For the pure 1 M LiDFOB half-cell, the lithium plating/stripping Coulombic efficiency becomes unstable after only 15–20 cycles, while the 0.6 M LiDFOB 0.6 M $LiBF_4$ shows not only higher Coulombic efficiency but also much more stable operation. Additionally, the half-cell voltage response

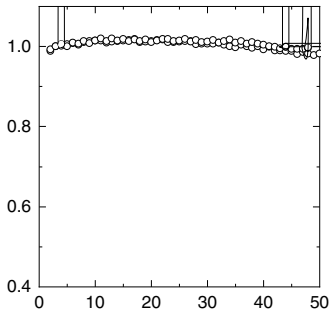

(Supplementary Fig. 3) shows that, while the pure and mixed LiDFOB are initially very similar, after repeated cycling the pure LiDFOB electrolyte demonstrates much larger polarization during lithium stripping. The maximum potential of these half-cells is limited to 1.0 V, so there is no high-voltage enhancement for the pure LiDFOB and it performs poorly, much as in the full cells with a lower upper cut-off voltage. These results provide further evidence that the LiDFOB/$LiFB_4$ combination is a more practical electrolyte for anode-free cells.

Li morphology and cell performance at increased pressure

Figure 2a shows capacity retention versus cycle number for the single-salt 1 M $LiPF_6$ (orange squares) and dual-salt 0.6 M LiDFOB 0.6 M $LiBF_4$ (blue circles) electrolytes under varying applied pressure. Cells with 1 M $LiPF_6$ constrained under low pressure (~kPa) have very poor capacity retention (orange, closed squares). Previous reports have demonstrated the ability of increased stack pressure to improve lithium-metal cycling efficiency[19,20,32–34], and here increasing the stack pressure of the $LiPF_6$ cell to 1,200 kPa (orange, open squares) more than triples the number of cycles before the cells lose 60% of the initial capacity. The test fixture used to apply pressure to the pouch cells is shown in Supplementary Fig. 4. The application of mechanical pressure affects the lithium morphology, which can reduce capacity loss in two ways: (1) less dendritic lithium forms, less unusable electrically isolated metallic lithium, and (2) lower surface-area lithium minimizes the reactions with electrolyte that consume active lithium to form a solid electrolyte interphase (SEI). Scanning electron microscopy (SEM) images of lithium morphology taken in the fully charged state (4.5 V) are shown in Fig. 2b–m. Comparable optical images are shown in Supplementary Fig. 6. Fig. 2b,c shows that lithium metal plated in the $LiPF_6$ electrolyte under low pressure is dendritic and has high surface area. Increasing stack pressure improves capacity retention by initially resulting in a more compact lithium surface after one charge (Fig. 2d), and destroying the dendrite formation after 50 cycles (Fig. 2e).

Figure 2f shows that the dual-salt LiDFOB/$LiBF_4$ electrolyte results in a dendrite-free morphology even under low pressure, which is expected given the improved capacity retention shown in Fig. 2a (blue, closed circles). Even after 50 cycles, the morphology remains mostly compact (Fig. 2g). Higher stack pressure only slightly improves capacity retention for the dual-salt LiDFOB/$LiBF_4$ electrolyte; cells at 50 cycles with this electrolyte show about 95% capacity retention when cycled at ~kPa and about 97% capacity retention when cycled at about 1,200 kPa (Fig. 2a, blue circles). With extended cycling, the dual-salt electrolyte under high stack pressure reaches 90 cycles at 80% capacity retention (Supplementary Fig. 7). The lithium in the dual-salt LiDFOB/$LiBF_4$ cells is close packed and dendrite free for both low- and high-pressure cells after one charge (Fig. 2f,h) and very flat after 50 cycles (Fig. 2g,i–m). In fact, the quality of the lithium shown for the dual-salt LiDFOB/$LiBF_4$ electrolyte under 1,200 kPa shown in Fig. 2i represents the flattest and most dendrite-free lithium after 50 cycles in a non-aqueous liquid electrolyte of which the authors are aware. Figure 2j–m shows that this dual-salt electrolyte under 1,200 kPa results in a smooth lithium mosaic comprised of densely packed lithium domains up to 50 μm in diameter. In addition to these images taken at the top of charge with the maximum amount of lithium plated, images were taken at an intermediary state of charge with most (~80%) of the lithium stripped away to confirm that this highly desirable lithium morphology persists throughout the thickness of the plated lithium. Supplementary Fig. 8 shows that even when most of the lithium is stripped away the morphology still consists of large ~50 μm domains, revealing that the internal structure of the plated lithium is consistent with the surface morphology. This suggests that the tightly packed domains achieved with LiDFOB/$LiBF_4$ electrolyte under 1,200 kPa shown in Fig. 2j–m are in fact lithium columns. Similar smooth lithium morphology is seen on the first cycle for cells that only use LiDFOB but have the same total salt concentration (Supplementary Fig. 9), which makes sense given the similar capacity retention for 1 M cells cycled to 4.5 V with these two electrolytes (Fig. 1c,d). For LiDFOB cells cycled to lower voltage (4.3 V, 4.2 V in Fig. 1c,d) or with lower salt concentration (1 M LiDFOB in Fig. 1b), it is expected that the poorer capacity retention would also result in worse lithium morphology. Demonstrating that such high-quality lithium can be created with a liquid electrolyte may eventually eliminate any need for solid-state cells.

The anode electrolyte interphase

Since the lithium morphology is greatly improved by changing only the salt used in the electrolyte, the difference in SEI composition was

explored. Figure 3 shows results from surface analysis by X-ray photoelectron spectroscopy (XPS) of the negative electrode from anode-free pouch cells with three different electrolytes. Measurements were made after one C/5 charge C/2 discharge cycle (3.5–4.5 V) at 40 °C and 75 kPa stack pressure. Each spectrum corresponds to an electrode formed in a different electrolyte: black—1 M $LiPF_6$, blue—1 M LiDFOB and green—0.6 M LiDFOB 0.6 M $LiBF_4$. All electrolytes use an FEC:DEC (volume ratio 1:2) solvent mix. The sampling depth with this technique is 2–5 nm. In each region, spectra are normalized to the highest intensity and a Shirley-type background is subtracted. Spectra are offset for clarity. Assignments of components by binding energy are from the NIST XPS database[28] as well as other research papers[21,35].

The fluorine 1s spectra in Fig. 3a contain one component at 685 eV assigned to lithium fluoride (LiF) and a second component at higher binding energy that is broadly assigned to organic oxygen-, carbon-, boron- and fluorine-containing components, which may be similar to the LiDFOB decomposition products proposed by Schedlbauer *et al.*[29]. The SEI formed with LiDFOB (green) has a higher ratio of organic fluorine components relative to LiF, whereas the SEI formed with $LiPF_6$ has more LiF relative to organic components. The increased organic component may contribute to the improved lithium morphology and cycling efficiency in the single-salt LiDFOB cells. The SEI formed in the dual-salt LiDFOB–$LiBF_4$ electrolyte has a large contribution from both organic fluorine components and LiF. Other researchers speculated that large amounts of LiF in the SEI are favourable for good lithium plating[27]. Note that only information about the relative composition of the SEI is known from these data, not the absolute amount of LiF present. Here, the cells with the best capacity retention have an SEI composed of both organic components and LiF. Oxygen 1s and carbon 1s spectra are shown in Fig. 3b,c, respectively, to further highlight the different organic SEI components formed in the three electrolytes. Electrolyte salts react at both the negative and positive electrodes, as indicated by the presence of boron (for LiDFOB and $LiBF_4$ electrolytes) or phosphorus (for $LiPF_6$ electrolytes). B and P spectra are shown in Supplementary Fig. 10. Positive-electrode XPS analysis is shown in Supplementary Fig. 11.

Electrolyte consumption

Figure 4 shows NMR measurements of electrolyte composition during cycling for anode-free cells that started with three different electrolytes: 0.9 m (1 M) $LiPF_6$ (a,b), 0.9 m (1 M) LiDFOB (c,d) and 0.5 m (0.6 M) LiDFOB–0.5 m (0.6 M) $LiBF_4$ (e,f). All electrolytes used FEC:DEC (44:56 weight ratio, 1:2 volume ratio) solvent, and cycling conditions were the same as for the cells in Fig. 1: 40 °C, C/5 charge, C/2 discharge between 3.6 and 4.5 V at 75 kPa.

To accurately capture the trends in electrolyte composition with cycle number, the composition at cycle zero is measured by NMR from electrolyte extracted from a cell after filling and wetting. Measurements made for subsequent cycles use the same method as for cycle zero. Supplementary Table 1 compares the composition as measured on cycle zero with the composition calculated from the mass of each component mixed into the electrolyte. For each electrolyte, the salt concentration measured on cycle zero is higher than the salt concentration measured just after formation (cycle 1). Some salt may be consumed during the first charge cycle to form the initial SEI, which is also indicated by the presence of boron (for LiDFOB and $LiBF_4$ electrolytes) or phosphorus (for $LiPF_6$ electrolytes) on the electrode surface after formation (measured by XPS; Supplementary Fig. 10). After formation, the cells with $LiPF_6$ (Fig. 4a) maintain the same salt concentration during cycling, despite the fact that they have less than 20% capacity remaining at cycle 20. Not much salt is consumed in this system, and although the composition of the solvent shifts to slightly higher FEC content (Fig. 4b) the amounts of electrolyte measured at cycle 1 and cycle 20 are similar (Supplementary Fig. 12). The primary cause of capacity loss in this system is probably not from the consumption of lithium to form an SEI, since this would also consume electrolyte. Instead, these cells must lose most of their capacity from the formation of isolated metallic lithium, which is likely given the highly dendritic lithium morphology (Fig. 2b,c). In contrast, both LiDFOB and $LiBF_4$ are consumed during cycling for cells that use single- or dual-salt electrolytes (Fig. 4c,e

NMR measurements on cells that started with pure 1M LiDFOB electrolytes show that when LiDFOB is consumed a small amount of $LiBF_4$ is formed (Fig. 4c and Supplementary Fig. 14). Recall from Fig. 1c that, for cells with single-salt LiDFOB electrolyte, capacity retention versus cycle number improved with higher upper cut-off voltage. The best capacity retention was for the cells cycled up to 4.5 V. It is likely that higher voltage increases the amount of $LiBF_4$ formed, which then improves performance by turning the electrolyte into a dual-salt LiDFOB–$LiBF_4$ composition.

In addition to cell failure due to complete consumption of the salt in the electrolyte, the capacity retention in anode-free cells may be affected by changing electrolyte transport properties as the salt concentration decreases. Not only will electrolytes that start with different lithium salts have different SEI compositions, but the electrolyte transport properties will also be different. Previous researchers have shown that properties such as electrolyte diffusion can have a big effect on lithium morphology[26]. The transport properties of electrolytes used in this work have not yet been explored.

Conclusions

Anode-free pouch cells with zero excess lithium were tested with FEC:DEC-based liquid electrolytes using different lithium salts: $LiPF_6$, $LiBF_4$ and LiDFOB. Cells with a dual-salt LiDFOB–$LiBF_4$ electrolyte had the best performance of all the electrolytes tested—80% of the original capacity was retained for 90 cycles, which is an impressive cycle life for cells with no excess lithium. All previous reports of anode-free cells with liquid electrolytes fall below 80% capacity retention by 40 cycles or fewer[11,22,23]. SEM images of the lithium revealed flat, mosaic-like lithium morphology comprised of densely packed lithium columns with large domains up to 50 μm in diameter, which are desirable to prevent the formation of isolated metallic lithium and to reduce the reaction rate of lithium with the electrolyte by minimizing the surface area. This highly desirable lithium morphology in the dual-salt electrolyte may be influenced by the type of SEI formed compared with other electrolytes. XPS was used to show a dramatically different composition of the anode SEI formed in LiPF

accelerating voltage and 25 nm resolution). To prepare samples for SEM, cells were dissected in an argon-atmosphere glovebox and electrode pieces were rinsed with dimethyl carbonate (DMC) to remove residual salt. Dried samples were mounted on SEM stubs with conductive carbon tape. Samples were transferred from the glovebox to the scanning electron microscope in an argon-filled bag, and were briefly exposed to air for less than 30 s when loading in the scanning electron microscope.

Electrode surface analysis. SEI composition was analysed by XPS. Cells were formed at 40 °C by holding at 1.5 V for 24 h, charging at C/5 to 4.5 V, then discharging at C/2 to 3.0 V. After formation, cells were fully discharged to about 0.2 V before dissecting in an argon glovebox to harvest electrode samples. Each electrode piece was rinsed with ethyl methyl carbonate to remove any residual lithium salt. After drying, electrodes were mounted on XPS sample holders using ultrahigh-vacuum-compatible copper tape (3M). Electrodes were moved from the glovebox to the XPS system without exposing to air using a custom transfer suitcase. A SPECS spectrometer with a PHOIBOS 150 hemispherical analyser was used for XPS analysis with Mg K radiation (1,253.6 eV) under ultrahigh-vacuum conditions (2 10 ^{9} mbar). See ref. [38] for further details.

Electrolyte extraction. Electrolyte was extracted from cells in one of two ways. (1) Cells were cut open in a glovebox and filled with 1 ml of anhydrous deuterated DMSO (d-DMSO, Sigma). The solvent was massaged into the jelly roll, and then the electrolyte/d-DMSO mix was collected for analysis by NMR. (2) Cells were cut open outside the glovebox and the jelly roll was moved to a perfluoroalkoxy alkane vial with 10 g of DMC (BASF). Vials were sonicated for 10 min, mixed on a wrist-action shaker for 1 h, sonicated for 10 min, mixed on a wrist-action shaker for 1 h, sonicated for 10 min then mixed on a wrist-action shaker overnight. 100 mg of the DMC/electrolyte mix was added to about 0.8 ml of anhydrous d-DMSO for NMR analysis. Method 1 gives the salt concentration and relative percentages of electrolyte components that were in the pouch cell. Method 2 is a total extraction method and gives the salt concentration and total mass of each electrolyte component present in the pouch cell. The cells in Fig. 4a–d were analysed using method 2, which gives the composition (shown in Fig. 4b,d) and total amount of electrolyte (shown in Supplementary Fig. 11). The cells in Fig. 4e,f were analysed using method 1, which gives the salt concentration and relative solvent composition.

Electrolyte analysis. Electrolyte samples prepared in d-DMSO (as described in the previous section) were analysed using liquid NMR on a Bruker AV500 spectrometer. Proton (^{1}H) spectra were collected over the range 0–9 ppm. Fluorine (^{19}F) spectra were collected with no background suppression over the range 200 to 0 ppm. Peaks for each solvent component appear in the ^{1}H spectrum at 6.7 ppm, 6.5 ppm and 4.7 ppm (FEC), 3.7 ppm (DMC), and 4.2 ppm and 1.2 ppm (DEC). Peaks for FEC and fluorine salts appear in the ^{19}F spectrum at the following chemical shifts: 123 ppm (FEC), 70 ppm ($LiPF_6$), 151 ppm (LiDFOB) and 148 ppm ($LiBF_4$). Peak assignments were confirmed from the ^{1}H and ^{19}F spectra of each pure component.

Peak areas from the ^{1}H spectrum were used to calculate the relative FEC:DEC composition. For electrolyte extracted by method 2 the amount of DMC present in the NMR sample was known, so the DMC signal was used as a standard to calculate the masses of FEC and DEC extracted from the pouch cell. The peak areas from the ^{19}F spectrum were used to calculate the salt amount relative to FEC, which was used with the information from the

elal8(le co(g t)6(o)4.0999999(e)]TJ2(t)-6(hi)12(um s)-6et)-5.9000001(h)4((l ext)-e)-5(c)-6.9000001(t)-5(r)13(o)-9(de p)12or

35. Naumkin, A. V., Kraut-Vass, A., Gaarenstroom, S. W. & Powell, C. J. NIST X-ray Photoelectron Spectroscopy Database Version 4.1. (National Institute of Standards and Technology, 2012); https://doi.org/10.18434/T4T88K
36. Bai, P., Li, J., Brushett, F. R. & Bazant, M. Z. Transition of lithium growth mechanisms in liquid electrolytes. Energy Environ. Sci. 9, 3221–3229 (2016).
37. Li, J. et al. Comparison of single crystal and polycrystalline $LiNi_{0.5}Mn_{0.3}Co_{0.2}O_2$ positive electrode materials for high voltage Li-ion cells. J. Electrochem. Soc. 164, A1534–A1544 (2017).
38. Madec, L. et al. E ect of sulfate electrolyte additives on $LiNi_{1/3}Mn_{1/3}Co_{1/3}O_2$/graphite pouch cell lifetime: correlation between XPS surface studies and electrochemical test results. J. Phys. Chem. C 118, 29608–29622 (2014).

Acknowledgements

This research was financially supported by Tesla Canada and NSERC under the Industrial Research Chairs Program. A.J.L. thanks the Nova Scotia Graduate Scholarship programme and the Walter C. Sumner Memorial fellowship for support. M.G. thanks the NSERC PDF Program. The authors acknowledge Dr J. Li (formerly of BASF) and Dr D. J. Xiong (formerly of Capchem) for providing chemicals used in the electrolytes, as well as S. Trussler for expert fabrication of the parts used in this work.

Author contributions

R.W., M.G., A.J.L. and J.R.D. conceived the idea. R.W., M.G. and A.J.L. designed the experiments with the guidance of J.R.D.; R.W., M.G. and A.J.L. performed the electrochemical measurements with assistance from S.H. and C.M.; R.W. performed the NMR analysis; R.W. performed the XPS analysis with guidance from I.G.H; M.G. and A.J.L. performed the SEM analysis; A.J.L. performed the mechanical pressure measurements. R.W., M.G., A.J.L. and J.R.D. prepared this manuscript with input from all other co-authors.

Competing interest

Rochelle Weber is employed by Tesla Canada R&D.

Additional information

Supplementary information is available for this paper at https://doi.org/10.1038/s41560-019-0428-9.

Reprints and permissions information is available at www.nature.com/reprints.

Correspondence and requests for materials should be addressed to J.R.D.

Publisher's note: Springer Nature remains neutral with regard to jurisdictional claims in published maps and institutional affiliations.